3.3 Large x, small x, lattice and machine learning

The edges of the kinematic plane, first-principles input, and the tools.

1. Where the standard framework is stressed

Every prediction in a fit of parton distribution functions (PDFs) has the form derived in chapters 1.4 to 1.6: distributions evolved by DGLAP and folded with a hard cross-section computed to a fixed order in α_S. For F_2, with what this form leaves out written last,

$$F_2(x,Q^2) = x\sum_a \big(C_a \otimes f_a\big)(x,Q^2)\Big|_{\text{fixed order}} + O\Big(\frac{M^2}{Q^2},\frac{\Lambda^2}{Q^2}\Big) + (\text{logarithms not summed}). \tag{3.3.1}$$

C_a are the coefficient functions, f_a the distributions, M the proton mass and Λ a hadronic scale of a few hundred MeV. The power terms are small when Q^2 is large, and the unsummed logarithms when x is close to neither 1 nor 0. This chapter goes to the places where those conditions fail, and then to two sources of help.

1. **Large** x (sections 2 to 4). The data lie at low Q^2 and low hadronic mass, so the power terms matter. The target-mass correction is derived; the deuteron, the ratio d/u and the logarithms of $1-x$ follow.
2. **Small** x (sections 5 and 6). Powers of $\alpha_S \ln(1/x)$ appear at every order. Their leading sum is derived and has a singularity that no fixed order contains.
3. **Lattice QCD** (section 7). A first-principles calculation of the same distributions.
4. **Machine learning and tools** (sections 8 and 9). The fit as a learning problem, and the interpolation grid, which is derived.

The Snowmass report [3] is the guide to the present state of each topic, ESW [1] to the small-x theory and Moore's thesis [2] to the methodology. Chapter 1.5 derived the large-x exponent, listed the small-x towers and introduced FK tables; those results are used here and not repeated.

2. Large x: the proton mass

This section derives how the proton mass changes the parton-model formula. The result has no free parameters.

Why large x means low hadronic mass

The invariant mass W of the hadronic final state is fixed by x and Q^2 (chapter 1.1):

$$W^2 = M^2 + Q^2\,\frac{1-x}{x}, \qquad W^2 \geq W_{\text{cut}}^2 \iff Q^2 \geq \big(W_{\text{cut}}^2 - M^2\big)\frac{x}{1-x}. \tag{3.3.2}$$

At fixed Q^2, raising x lowers W towards the resonances and the elastic point $W = M$. The Snowmass report states the consequence: few data constrain $x > 0.5$, much of what exists lies at low Q near the lower boundary of perturbation theory, and nuclear, target-mass and higher-twist corrections all enter there [3].

The kinematics with a massive target

Keep the struck quark massless, as in the parton model, but give the proton its mass. With the light-like vectors p and n of Eq. (1.4.2), a proton of mass M and a photon collinear with it are

$$P^\mu = p^\mu + \frac{M^2}{2}\, n^\mu, \qquad q^\mu = -\xi\, p^\mu + \frac{Q^2}{2\xi}\, n^\mu. \tag{3.3.3}$$

The quark carries momentum $k = \xi p$: a fraction ξ of the proton's light-cone momentum $n \cdot P$. The form of q is fixed by $q^2 = -Q^2$ and by the requirement that the quark is massless after the collision, $(\xi p + q)^2 = 0$. Computing $\nu = P \cdot q$ from Eq. (3.3.3) and using $x = Q^2/2\nu$ gives (derivation D1)

$$\xi = \frac{2x}{1+r}, \qquad r = \sqrt{1 + \frac{4x^2M^2}{Q^2}}. \tag{3.3.4}$$

This is the *Nachtmann variable*. Chapter 1.2 met the same expression from a cruder model in which the parton carried a fraction of the proton's mass. Here it is the light-cone momentum fraction of a massless quark, expressed through the measured x and Q^2. The quark distribution is a function of the light-cone fraction (chapter 1.3, section 7), so ξ and not x belongs in its argument.

The structure functions

Repeating the parton-model calculation with the vectors of Eq. (3.3.3) and projecting with the massive form of the hadronic tensor (chapter 1.1, section 6) gives (derivation D1)

$$F_2^{\mathrm{TM}}(x,Q^2) = \frac{x}{\xi\, r^2}\, F_2^{(0)}(\xi), \qquad 2x\, F_1^{\mathrm{TM}}(x,Q^2) = \frac{x}{\xi}\, F_2^{(0)}(\xi), \qquad F_L^{\mathrm{TM}} = 0. \tag{3.3.5}$$

Here $F_2^{(0)}(\xi) = \xi \sum_q e_q^2\, q(\xi)$ is the massless parton-model function of Eq. (1.4.1) evaluated at ξ, and F_L is the general form $r^2F_2 - 2xF_1$ of chapter 1.1, section 6. Three things follow.

- **The argument shifts.** $\xi < x$, and the distributions fall steeply at large x, so $F_2^{(0)}(\xi) > F_2^{(0)}(x)$. The shift, $\xi/x = 1 - x^2M^2/Q^2 + \ldots$, is largest at large x and low Q^2.
- **The prefactor works the other way.** $x/\xi r^2 < 1$. At moderate x the two effects nearly cancel; at large x the shift wins.
- **The Callan–Gross relation survives** in the form $r^2F_2 = 2xF_1$.

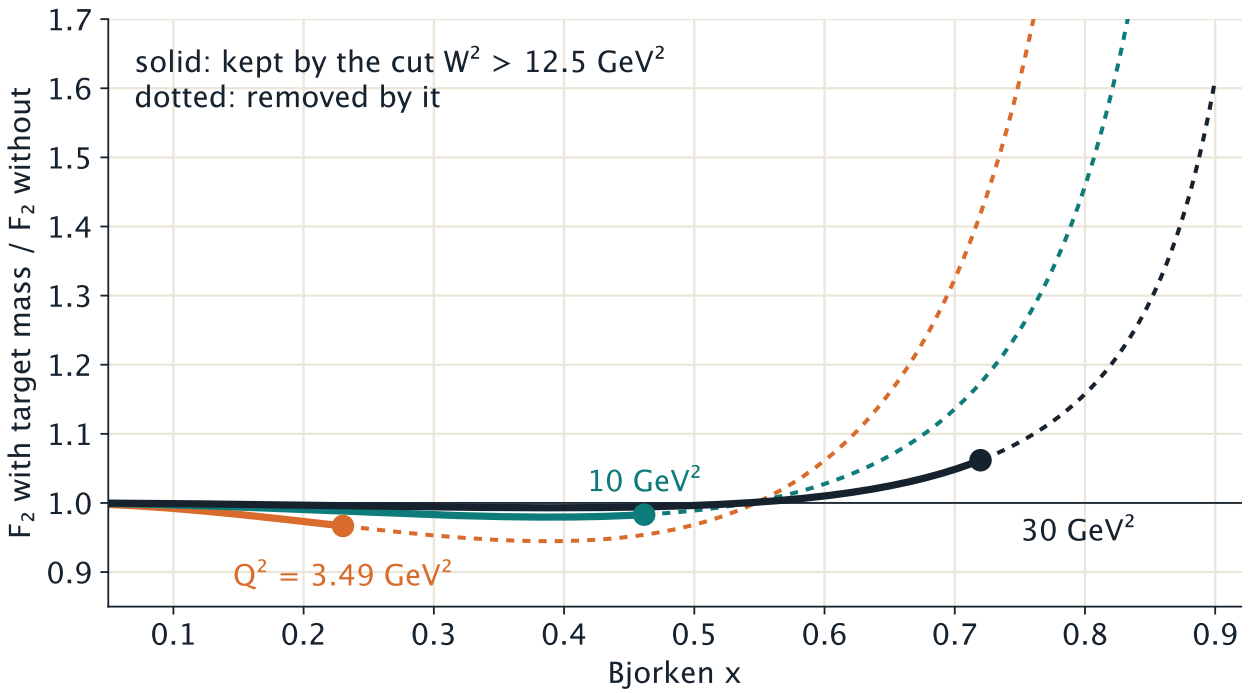

Figure 1. The target-mass ratio $F_2^{\mathrm{TM}}/F_2^{(0)}(x)$ from Eq. (3.3.5), for the toy shape $F_2^{(0)} \propto x^{1/2}(1-x)^3$ (illustrative). Solid lines: points with $W^2 > 12.5\ \mathrm{GeV}^2$. Dotted: points that the cut removes. The circle marks where each curve meets the cut.

BJORKEN X	W² ON THE Q² CUT	RATIO ON THE Q² CUT	Q² NEEDED TO PASS THE W² CUT	RATIO THERE
0.5	4.37	0.968	11.6	0.991
0.7	2.38	1.324	27.1	1.053
0.75	2.04	1.613	34.9	1.076

The cuts are $Q^2 > 3.49\ \mathrm{GeV}^2$ and $W^2 > 12.5\ \mathrm{GeV}^2$, the units are GeV², and the numbers are for the toy shape. The cut on W^2 removes the region where the correction is tens of per cent and leaves a few per cent at the largest surviving x. That is still larger than the errors of the best data, so the correction is applied.

Where the formula fails

At the elastic point $x = 1$ the Nachtmann variable is below 1:

$$\xi\big|_{x=1} = \frac{2}{1+\sqrt{1+4M^2/Q^2}} = 0.84 \quad \text{at } Q^2 = 4\ \mathrm{GeV}^2. \tag{3.3.6}$$

A distribution that vanishes at $\xi = 1$ is therefore not zero at $x = 1$, and Eq. (3.3.5) predicts inelastic scattering where only elastic scattering is possible. Close to threshold the final state is not a free quark, and the other power corrections are as large. Equation (3.3.5) is also not the only treatment: the prefactor depends on how the partons' transverse momentum and virtuality are handled. The variable ξ is common to all treatments.

3. Large x: higher twist, the deuteron and the down quark

This section covers the large-x corrections that kinematics does not fix, and shows why they limit knowledge of the d quark.

Higher twist

The factorised formula is the first term of an expansion in inverse powers of Q^2:

$$F_2(x,Q^2) = F_2^{\mathrm{LT}}(x,Q^2) + \frac{H(x)}{Q^2} + O\Big(\frac{1}{Q^4}\Big). \tag{3.3.7}$$

F_2^{LT} is the *leading-twist* part, built from single-parton distributions. $H(x)$ is the *higher-twist* (twist-four) term. It comes from processes in which more than one parton takes part in the hard scattering, and it is suppressed by a power of the hard scale (Moore, section 1.1.7 [2]). It is not expressible through the PDFs, so it must be fitted, modelled or cut away. The Snowmass report says that these effects can be significant for $W^2 \leq 15$–$20\ \mathrm{GeV}^2$, and that a distortion absorbed into the PDFs at low Q and large x is carried by evolution to smaller x at electroweak scales, where it can matter at the per-cent level [3].

The deuteron is not a proton plus a neutron

The d quark at large x is measured through the neutron, and the neutron through the deuteron (chapter 1.2). Write the deuteron structure function per nucleon as

$$F_2^{d}(x,Q^2) = c(x,Q^2)\ \tfrac{1}{2}\big[F_2^{p}(x,Q^2) + F_2^{n}(x,Q^2)\big]. \tag{3.3.8}$$

The factor c is the *nuclear correction*. It would be 1 for two free nucleons at rest; binding and the motion of the nucleons change it. The Snowmass report records that deuteron corrections can be sizeable and that the groups treat them differently: some apply a correction, as MSHT20 does, and some assign an uncertainty, as NNPDF4.0 does [3, 4, 5]. The CJ fits also apply a correction [4].

From the measured ratio to d/u

At large x the sea is negligible and the ratio $R = F_2^n/F_2^p$ depends only on d/u. With isospin symmetry, $F_2^p \propto 4u + d$ and $F_2^n \propto 4d + u$, so

$$R = \frac{1 + 4\,d/u}{4 + d/u}, \qquad \frac{d}{u} = \frac{4R - 1}{4 - R}. \tag{3.3.9}$$

R runs from $\frac{1}{4}$ at $d/u = 0$ to $\frac{2}{3}$ at $d/u = \frac{1}{2}$, the value for two u and one d quark with the same shape. The lower end is the bound of chapter 1.2.

An error in the nuclear correction moves R, and the map from R to d/u magnifies it. At fixed measured F_2^d and F_2^p (derivation D2),

$$\frac{\delta(d/u)}{d/u} = -\,\frac{15\,(1+R)}{(4-R)^2\ d/u}\ \frac{\delta c}{c}. \tag{3.3.10}$$

For $d/u = 0.2$ the coefficient is 8.4, and for $d/u = 0.1$ it is 15. A one per cent uncertainty on the deuteron correction is an 8 to 15 per cent uncertainty on d/u where d/u is small. This is why the d quark at large x is known less well than the u quark. The Snowmass report lists two ways round it at the Electron–Ion Collider: charged-current scattering

with positrons, which probes d-type quarks in the proton itself, and deuteron scattering in which a slow spectator proton tags a nearly free neutron [3].

The limit of x near one

Parametrisations give each distribution its own power, $u \propto (1-x)^{\beta_u}$ and $d \propto (1-x)^{\beta_d}$ (chapter 2.1). Then

$$\frac{d}{u} \;\propto\; (1-x)^{\beta_d-\beta_u}, \qquad \beta_{\text{eff}}(x,Q) \equiv \frac{\ln f(x,Q)}{\ln(1-x)}. \tag{3.3.11}$$

Unless the two exponents are equal, the ratio is forced to zero or to infinity at $x=1$. Where there are no data, the limit of d/u in a fit is an assumption of the functional form. Evolution does not change the difference: by the large-x result of chapter 1.5, section 8, both exponents grow by the same Δ.

Quark counting rules and several non-perturbative approaches predict $\beta \gtrsim 3$ for baryons, a behaviour expected only at $x \gtrsim 0.9$, where higher twist and threshold logarithms also act [3]. The Snowmass report warns against reading a fitted β as a test of this, because the nominal exponent is not unique (different functional forms can mimic one another), and recommends comparing the effective exponent β_{eff} of Eq. (3.3.11), which tends to β as $x \to 1$. It leaves open how far such expectations should shape a fit, given the bias they introduce [3].

---

4. Large x: threshold logarithms

This section shows where logarithms of $1-x$ come from in a coefficient function and how large they are.

Chapter 1.6, section 5, found, in the $\overline{\text{MS}}$ quark coefficient function, the terms $2C_F\big[\ln(1-z)/(1-z)\big]_+$ and $-\frac{3}{2}C_F\big[1/(1-z)\big]_+$. They are what is left when the soft-gluon divergences of real and virtual emission cancel. Near $z=1$ the final state has just enough energy to be produced, hence *threshold* logarithms. Their size is clearest in moments, where large N corresponds to large x. With the harmonic sums $S_1(n)=\sum_{k=1}^{n}1/k$ and $S_2(n)=\sum_{k=1}^{n}1/k^2$ (derivation D3),

$$\begin{aligned} \int_0^1 dz\; z^{N-1}\Big[\frac{1}{1-z}\Big]_+ &= -S_1(N-1), \\ \int_0^1 dz\; z^{N-1}\Big[\frac{\ln(1-z)}{1-z}\Big]_+ &= \tfrac{1}{2}\Big[S_1^2(N-1)+S_2(N-1)\Big]. \end{aligned} \tag{3.3.12}$$

At large N, $S_1(N-1)\to\ln\bar N$ with $\bar N = N e^{\gamma_E}$, and $S_2\to\pi^2/6$. The moments of the coefficient function, in the normalisation $C_q(N)=1+\frac{\alpha_S}{2\pi}C_q^{(1)}(N)$, then become (derivation D3)

$$C_q^{(1)}(N) \;\xrightarrow{N\to\infty}\; C_F\Big[\ln^2\bar N + \tfrac{3}{2}\ln\bar N - \tfrac{9}{2} - \tfrac{\pi^2}{6}\Big]. \tag{3.3.13}$$

Numbers. For $\alpha_S=0.2$ the exact first-order correction $\frac{\alpha_S}{2\pi}C_q^{(1)}(N)$ is 0.14 at $N=5$, 0.31 at $N=10$ and 0.53 at $N=20$. The double logarithm alone gives 0.54 at $N=20$. A first-order term that is half the leading one is not a small correction.

The pattern repeats. Each further soft gluon can bring two more logarithms, so that

$$C_q(N) = 1 + \sum_{n\ge 1}\alpha_S^n \sum_{m=0}^{2n} c_{nm}\,\ln^m\bar N. \tag{3.3.14}$$

When $\alpha_S \ln^2 \bar{N}$ is of order one, every order contributes equally. *Threshold resummation*, also called soft-gluon or large-x resummation, sums the towers of Eq. (3.3.14) to all orders to a stated logarithmic accuracy [3, 6]. The sources do not derive it, and neither does this chapter.

What matters for fits is in the Snowmass report [3]. The size of these terms differs between processes, so leaving them out distorts the PDFs. One set has been fitted with resummed hard cross-sections, using only deep inelastic, Drell–Yan and top-pair data, for which resummed calculations existed [6]. Its lesson is consistency: near threshold the resummed PDFs partly compensate the enhancement of the resummed hard cross-section, so the two should be used together. Far from threshold the two kinds of PDF agree. Global fits, including ours, are fixed order.

---

5. Small x: the sum of the leading logarithms

This section derives the all-order sum of the leading logarithms of $1/x$ in the gluon anomalous dimension, and shows that the sum has a singularity that no fixed order has.

Logarithms are poles at N = 1

Chapter 1.5 listed the towers: at order α_S^{n+1} the gluon splitting function contains terms up to $\frac{1}{x}\ln^n\frac{1}{x}$ (chapter 1.5, section 9). In moment space each is a pole,

$$\int_0^1 dx\; x^{N-1}\;\frac{1}{x}\,\frac{\ln^k(1/x)}{k!} = \frac{1}{(N-1)^{k+1}}. \tag{3.3.15}$$

At small x a fixed-order anomalous dimension is a polynomial in $1/(N-1)$. Whatever its order, its only singularity there is at $N=1$, and the gluon it produces grows more slowly than any power of $1/x$ (chapter 1.4).

The characteristic function

The terms with one logarithm per power of the coupling are summed by the BFKL equation (chapter 1.5) [7]. ESW solve it by a Mellin transform in the transverse scale, which in their derivation is the size of a colour dipole: a gluon density that depends on the scale as $(Q^2)^\gamma$ evolves in x as a pure power, $x^{-\bar{\alpha}_S\chi(\gamma)}$, with $\bar{\alpha}_S = C_A\alpha_S/\pi$ and (ESW Eqs. 4.217, 4.218)

$$\chi(\gamma) = 2\psi(1) - \psi(\gamma) - \psi(1-\gamma) = \frac{1}{\gamma} + 2\zeta(3)\,\gamma^2 + 2\zeta(5)\,\gamma^4 + \dots \tag{3.3.16}$$

ψ is the logarithmic derivative of the Gamma function and ζ the Riemann zeta function. χ is the *Lipatov characteristic function*. It is symmetric about $\gamma=\frac{1}{2}$, where it has its minimum $\chi(\frac{1}{2}) = 4\ln 2$.

The anomalous dimension to all orders

DGLAP evolution says the opposite thing in the opposite variable: a density that behaves as $x^{-(N-1)}$ evolves in the scale as $(Q^2)^{\gamma(N)}$, where $\gamma(N) = \frac{\alpha_S}{2\pi}\gamma_{gg}(N)$ at fixed coupling. Where both descriptions hold, the same function $x^{-(N-1)}(Q^2)^\gamma$ must satisfy both, which ties the two exponents together (derivation D4):

$$\bar{\alpha}_S\,\chi(\gamma) = N - 1. \tag{3.3.17}$$

Solving for γ as a series in $\bar{\alpha}_S/(N-1)$ with Eq. (3.3.16) gives (derivation D4)

$$\gamma(N) = \frac{\bar\alpha_S}{N-1} + 2\zeta(3)\Big(\frac{\bar\alpha_S}{N-1}\Big)^4 + 2\zeta(5)\Big(\frac{\bar\alpha_S}{N-1}\Big)^6 + 12\,\zeta(3)^2\Big(\frac{\bar\alpha_S}{N-1}\Big)^7 + \dots \tag{3.3.18}$$

The first term is the leading-order pole $2C_A/(N-1)$ of γ_{gg}. The second and third orders are absent. The fourth-order coefficient, in the normalisation of chapter 1.5, section 9, is $A_3^{(3)} = 2\zeta(3)(2C_A)^4/3! = 432\,\zeta(3) = 519.3$. ESW's Eq. (4.188) prints 518.4, with no formula. That is exactly 432×1.2, so the 0.2% difference is what rounding $\zeta(3) = 1.2021$ to 1.2 would give; ESW's text neither confirms nor excludes this. By Eq. (3.3.15) the series is, in x space,

$$\begin{aligned} x\,P_{gg}(x)\Big|_{\text{leading logs}} &= \bar\alpha_S\left[1 + \frac{2\zeta(3)}{3!}\,L^3 + \frac{2\zeta(5)}{5!}\,L^5 + \frac{12\,\zeta(3)^2}{6!}\,L^6 + \dots\right], \\ L &= \bar\alpha_S \ln\frac{1}{x}. \end{aligned} \tag{3.3.19}$$

Numbers. For $\bar\alpha_S = 0.2$ and $x = 10^{-4}$, $L = 1.84$ and the four terms are 1, 2.50, 0.37 and 0.94. The first correction, which appears only at order α_S^4, is two and a half times the leading term. That is the sense in which fixed order is unstable at small x: successive orders do not decrease.

The singularity

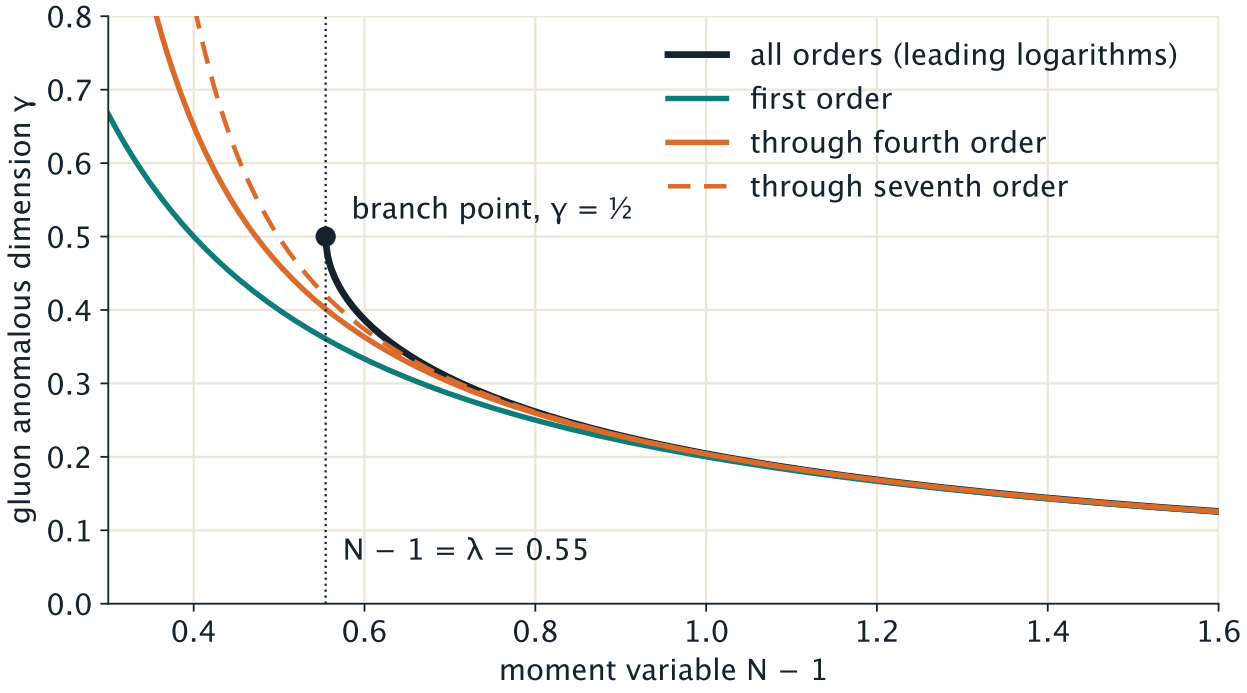

Figure 2. The leading-logarithm anomalous dimension for $\bar\alpha_S = 0.2$. Black: the solution of Eq. (3.3.17). Coloured: Eq. (3.3.18) cut off after one, four and seven orders. Every truncation is finite for all $N > 1$. The full sum ends at a branch point at $N - 1 = \lambda$.

χ has a minimum, so Eq. (3.3.17) has no real solution below a critical N:

$$N - 1 \;\geq\; \lambda = \bar\alpha_S\,\chi(\tfrac12) = 4\ln 2\;\bar\alpha_S, \qquad \gamma(1+\lambda) = \tfrac12. \tag{3.3.20}$$

Near the minimum χ is quadratic in $\gamma - \frac12$, so $\gamma(N)$ has a square-root branch point at $N = 1 + \lambda$. The rightmost singularity in N fixes the small-x behaviour: $x\,g \sim x^{-\lambda}$, the BFKL power of chapter 1.5, section 9. For $\bar\alpha_S = 0.2$, $\lambda =$

0.55; there the first-order truncation gives $\gamma = 0.36$ and the fourth-order one 0.40, against the true $\frac{1}{2}$. The series (3.3.18) converges only for $N - 1 > \lambda$. Fixed order sees the power $x^{-\lambda}$ as an endless sequence of logarithms.

> **Two limits, one pattern.** Near $x = 1$ the coefficient functions carry powers of $\alpha_S \ln^2 N$; near $x = 0$ the splitting functions carry powers of $\alpha_S \ln(1/x)$. In both, fixed order expands in a quantity that is not small, and the all-order sum differs in kind from any truncation. In between, where almost all data lie, fixed order is accurate and is what every global fit uses.

---

6. Small x: data, resummed fits and saturation

This section sets the theory of section 5 against what the data and the fits show.

What HERA showed

HERA collided electrons with protons at a centre-of-mass energy near 300 GeV and reached $x \sim 10^{-5}$ in the deep inelastic region. Two findings reported by ESW frame everything since [1].

- **Fixed order worked.** NLO fits described the small-x F_2 data very well, with F_2 rising roughly linearly in $\ln Q^2$. The double-logarithmic form of chapter 1.4 was tested directly: H1 data plotted against its scaling variable rose with slope $2.22 \pm 0.04 \pm 0.10$, against a predicted 2.4.
- **So did the alternative.** A BFKL-based form, $F_2 = C(Q^2)\, x^{-\lambda}$ with $\lambda \approx 0.5$ plus a constant background, also described the data.

ESW add that the leading logarithms are not the whole story. F_2 at small x evolves through $P_{qg} \otimes g$, and P_{qg} has no leading logarithms, so its formally subleading tower is what matters. And the leading-logarithm kernels violate momentum conservation.

Resummed fits

The modern resummation takes BFKL at next-to-leading logarithmic accuracy and matches it to collinear factorisation at NLO or NNLO [3]. Its numerical implementation in the public code HELL made a global fit possible.

- A fit to the NNPDF3.1 data set, with small-x logarithms summed in evolution and coefficient functions, found significant evidence for resummation in the HERA data at small x and low Q^2; an xFitter analysis reached a similar conclusion [8].
- The CT18X and CT18Z sets reach a similar χ^2 for the same data by a different route: a factorisation scale in deep inelastic scattering that depends on x, motivated by a saturation model [3].
- Both enhance the gluon at small x and low Q, the resummed fit more strongly. They agree on F_2 and pull F_L in different directions below $x = 10^{-4}$, so a measurement of F_L there would separate them.
- Hadron-collider cross-sections must also be resummed before such fits are fully consistent, and subleading terms are found to be larger than leading ones, so several towers are needed for quantitative control [3].

Forward physics

The smallest x in hadron collisions comes from production at large rapidity y, where the two partons have $x \sim (Q/\sqrt{s})\, e^{\pm y}$ [3]. For $Q = 5$ GeV and $y = 4.5$ at $\sqrt{s} = 13$ TeV (illustrative values) the smaller fraction is 4×10^{-6}. The

Snowmass report gives $x \sim 10^{-6}$ as the reach of LHCb data, where it expects resummation to matter most [3].

Saturation

Growth as a power of $1/x$ cannot continue. ESW's estimate treats the gluons as discs. A gluon probed at scale μ has transverse area of order $1/\mu^2$ and interacts with strength α_S. The gluons overlap, and recombination $gg \to g$ competes with splitting, when their total area reaches that of the proton (ESW Eq. 4.228):

$$\frac{\alpha_S(\mu^2)}{\mu^2}\, x\, g(x,\mu^2) \;\gtrsim\; \pi R^2, \qquad R \approx 5\ \text{GeV}^{-1}. \tag{3.3.21}$$

With $\pi R^2 = 78.5\ \text{GeV}^{-2}$, at $\mu^2 = 4\ \text{GeV}^2$ and $\alpha_S = 0.3$ this needs $x\, g \gtrsim 10^3$. ESW conclude that saturation is unlikely to play a major role in the HERA region [1]. The Snowmass report adds that the boundary between the resummation region and the saturation region is ambiguous, and that once saturation is reached collinear factorisation fails and a PDF is no longer a useful concept; in a nucleus of mass number A the effect is enhanced by $A^{1/3}$ [3].

---

7. Lattice QCD

This section explains what a lattice calculation can compute, how the x dependence is reached, and where the results stand.

The obstacle

Lattice QCD evaluates the path integral numerically on a grid in Euclidean space-time with spacing a, and takes $a \to 0$ [3]. Euclidean time is imaginary time. Correlators of fields at equal time are the same in both descriptions; correlators at different real times are not available. The quark distribution, as defined in chapter 1.3, section 7, needs two fields separated along the light cone, which means at different times. It cannot be computed directly.

The moments can be computed, because they are matrix elements (chapter 1.3, section 8) of local operators, with both fields at one point. A few low moments do not determine a function of x.

Space-like correlators

The route to the x dependence starts from a general property. Lorentz covariance restricts the matrix element of the two fields at any separation z to two scalar functions (derivation D5):

$$\langle P|\, \bar\psi(0)\, \gamma^\mu\, \mathcal{W}[0,z]\, \psi(z)\, |P\rangle = 2P^\mu\, \mathcal{M}(\nu, z^2) + z^\mu\, \mathcal{N}(\nu, z^2), \qquad \nu = P\cdot z. \tag{3.3.22}$$

$\mathcal{W}$ is the Wilson line of chapter 1.3, section 7, along the straight path. The invariant ν is called the *Ioffe time*. On the light cone, $z = \lambda n$, the definition of the distribution given there becomes (derivation D5)

$$q(x) = \int_{-\infty}^{\infty} \frac{d\nu}{2\pi}\, e^{i\nu x}\, \mathcal{M}(\nu, 0). \tag{3.3.23}$$

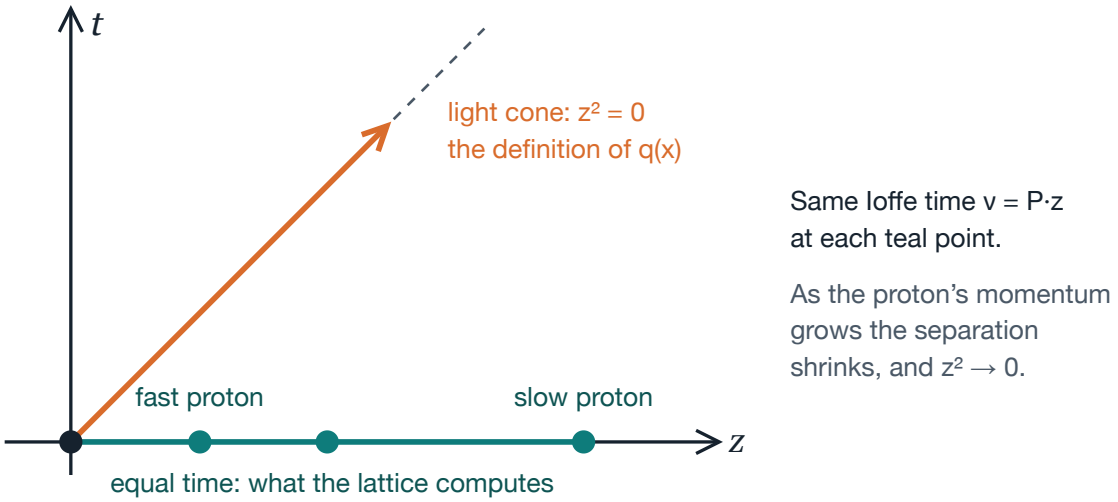

Figure 3. Two ways to separate the quark fields. The distribution is defined on the light cone (orange), which the lattice cannot reach. The lattice computes at equal time (teal). The function $\mathcal{M}(\nu, z^2)$ of Eq. (3.3.22) is common to both; the lattice knows it at $z^2 < 0$, and at fixed ν a larger momentum brings z^2 closer to zero.

On the lattice the separation is spatial, $z = (0, 0, 0, z_3)$, and the proton has momentum P_z along the same axis. The component $\mu = 0$ of Eq. (3.3.22) then gives $2E\,\mathcal{M}(\nu, -z_3^2)$ with $\nu = -P_z z_3$: the same function, at $z^2 = -z_3^2$ in place of zero. Two ways of using it are named in the Snowmass report [3, 9]:

$$\tilde{q}(y, P_z) = \int \frac{d\nu}{2\pi}\, e^{i\nu y}\, \mathcal{M}\Big(\nu, -\frac{\nu^2}{P_z^2}\Big), \qquad \mathcal{P}(y, z_3^2) = \int \frac{d\nu}{2\pi}\, e^{i\nu y}\, \mathcal{M}\big(\nu, -z_3^2\big). \tag{3.3.24}$$

The first is the *quasi-PDF*: the Fourier transform at fixed momentum. The second is the *pseudo-PDF*: the transform at fixed separation. Both reduce to $q(y)$ if $\mathcal{M}$ does not depend on its second argument.

Matching

$\mathcal{M}$ does depend on z^2: logarithmically at short distance, which is perturbative, and through power corrections. The quasi-PDF approach, large-momentum effective theory, relates quasi-PDFs at large but finite momentum to $\overline{\text{MS}}$ distributions through a factorisation theorem [3, 9]. Schematically,

$$\tilde{q}(y, P_z) = \int \frac{dx}{|x|}\, C\Big(\frac{y}{x}, \frac{\mu}{|x|P_z}\Big)\, q(x, \mu^2) + O\Big(\frac{\Lambda^2}{P_z^2}, \frac{M^2}{P_z^2}\Big). \tag{3.3.25}$$

This has the structure of Eq. (3.3.1): a calculable kernel C, the distribution, and power corrections, with the proton's momentum as the hard scale. Most calculations so far used the kernel at NLO; NNLO kernels exist [3].

Why the momentum must be large

The momentum also sets the resolution. If the correlator is known for separations up to $z_{\max}$, the Ioffe time reaches $\nu_{\max} = P_z z_{\max}$, and the transform (3.3.23) cut off there returns the distribution smeared over a width (derivation D5)

$$q_{\text{rec}}(x) = \int dx'\; q(x')\, \frac{\sin\big[\nu_{\max}(x - x')\big]}{\pi\,(x - x')}, \qquad \Delta x \approx \frac{\pi}{\nu_{\max}}. \tag{3.3.26}$$

The momenta in the calculations compared by the Snowmass report range from 1.4 to 3.3 GeV. With $P_z = 2.6$ GeV and $z_{\max} = 1$ fm (an illustrative choice), $\nu_{\max} = 13$ and $\Delta x \approx 0.24$. Structure at small x is the first thing lost. The report says the same from the lattice side: the small-x region and the antiquarks carry large systematic errors that only a larger P_z can remove, while a larger P_z raises the statistical noise [3].

Where it stands

All statements here are from the Snowmass report [3].

- **Isovector quarks.** $u - d$ is the most studied combination. One calculation has reached the continuum limit at physical pion mass, with three lattice spacings between 0.06 and 0.12 fm. Different calculations are in reasonable agreement with each other after their systematic errors are scaled up.
- **Strangeness.** For $s - \bar{s}$ at $x > 0.3$ the lattice uncertainty is small compared with that of the CT18As fit, and including the lattice points in that fit greatly reduced its uncertainty there. Lattice results serve as data for combinations that experiments constrain poorly.
- **Gluon.** Exploratory, mostly at pion masses above the physical one.
- **The coupling.** The lattice average is $\alpha_S(M_Z) = 0.1184(8)$. Our fits use 0.118.

In the other direction, the distributions from global fits are the benchmark against which lattice methods are validated [3].

---

8. Machine learning

This section states PDF fitting as a learning problem and lists where learning methods enter beyond the fit. Chapters 2.1, 2.3 and 2.4 covered the network, replicas, stopping and closure tests.

The fit as supervised regression

The Snowmass report calls PDF determination a problem “very well suited” to machine learning: the functional form is unknown, and there is agreement on the cost function [3]. With a network of weights w in place of a fixed form, the cost is the χ^2 of chapter 2.2 with the FK-table prediction of chapter 1.5, section 3:

$$\begin{aligned} \chi^2(w) &= \sum_{I,J} \left[D_I - T_I(w)\right] C_{IJ}^{-1} \left[D_J - T_J(w)\right], \\ T_I(w) &= \sum_{b,k} \mathrm{FK}_{I,bk}\; x_k f_b(x_k, Q_0^2; w). \end{aligned} \tag{3.3.27}$$

Three features separate this from textbook regression.

- **The target function is never observed.** The network output meets the data only after the FK convolution. Each point constrains an integral over a range of x and a mixture of flavours.
- **The uncertainty is the product.** A best-fit function without a faithful error band is of no use for a measurement. Hence replicas and closure tests.
- **Extrapolation matters.** Where there are no data the result reflects the prior built into the method (chapter 2.1).

The architecture, optimiser and stopping rule are hyperparameters. NNPDF4.0 fixes them by an automatic scan and minimises by gradient descent, where earlier releases used trial and error and a genetic algorithm [3, 10]. The same methods are used for nuclear PDFs and fragmentation functions [3].

Simultaneous fits

A prediction depends on more than the PDFs: on α_S, on electroweak parameters, and possibly on new physics. Fitting each with the other held fixed ignores their correlation. SIMUnet extends the NNPDF network by one further layer of trainable weights, so that PDFs and parameters are fitted on an equal footing [3, 11]. For Wilson coefficients c_n of an effective field theory the layer multiplies each Standard Model prediction by (Moore, Eqs. 4.8 and 4.9 [2])

$$T_I = T_I^{\mathrm{SM}}(w)\left[1 + \sum_n c_n\, R_I^{(n)} + \sum_{n\le m} c_n c_m\, R_I^{(n,m)}\right]. \tag{3.3.28}$$

The R_I are ratios of new-physics to Standard Model cross-sections, computed once. Chapter 3.2 takes up what such fits find.

Other uses

The Snowmass report lists four [3, 12]. A genetic algorithm *compresses* a set of Monte Carlo replicas to a smaller one with minimal loss of statistical information. A generative adversarial network enhances a set of replicas to reduce the finite-size artefacts of compression. Quantum machine-learning algorithms have been tried as the parametrisation. And in the CT18 analysis, networks model the dependence of the log-likelihood on the fit parameters, replacing exact evaluations in scans of a space of tens of dimensions.

---

9. Tools, and what an interpolation grid does

This section derives the grid representation of a convolution and places the public tools around it.

The problem

A hadron-collider cross-section at NNLO takes of order 10^5 CPU hours, and it is needed thousands of times, for different PDFs, values of α_S and scales [3]. The FK tables of chapter 1.5 are made from something more basic, the interpolation grid, which stores the hard cross-section before any PDF has been chosen.

The grid representation of a convolution

Take one parton and one scale first. The cross-section is $\sigma = \int_0^1 dx\, f(x)\,\hat\sigma(x)$, with $\hat\sigma$ the hard cross-section for the observable in question. Choose nodes $x_1, \dots, x_n$ and interpolating functions E_i, as in chapter 1.5, section 3:

$$f(x) \approx \sum_{i=1}^{n} f(x_i)\, E_i(x), \qquad E_i(x_j) = \delta_{ij}, \qquad \sum_i E_i(x) = 1. \tag{3.3.29}$$

Substituting, the PDF leaves the integral (derivation D6):

$$\sigma \approx \sum_{i=1}^{n} f(x_i)\; g_i, \qquad g_i = \int_0^1 dx\; E_i(x)\,\hat\sigma(x). \tag{3.3.30}$$

The numbers g_i are the *grid*. They depend on the process, the cuts and the bin, and not on the PDF.

In practice $\hat\sigma$ is produced by a Monte Carlo integration over the final state, as a stream of events $m = 1, \dots, N_{\mathrm{ev}}$, each with a momentum fraction x_m and a weight w_m. The grid is filled event by event (derivation D6):

$$g_i = \sum_{m=1}^{N_{\text{ev}}} w_m \, E_i(x_m). \tag{3.3.31}$$

Each event spreads its weight over the few nodes nearest to x_m [3]. The expensive calculation is run once, and Eq. (3.3.30) is then a sum over n numbers.

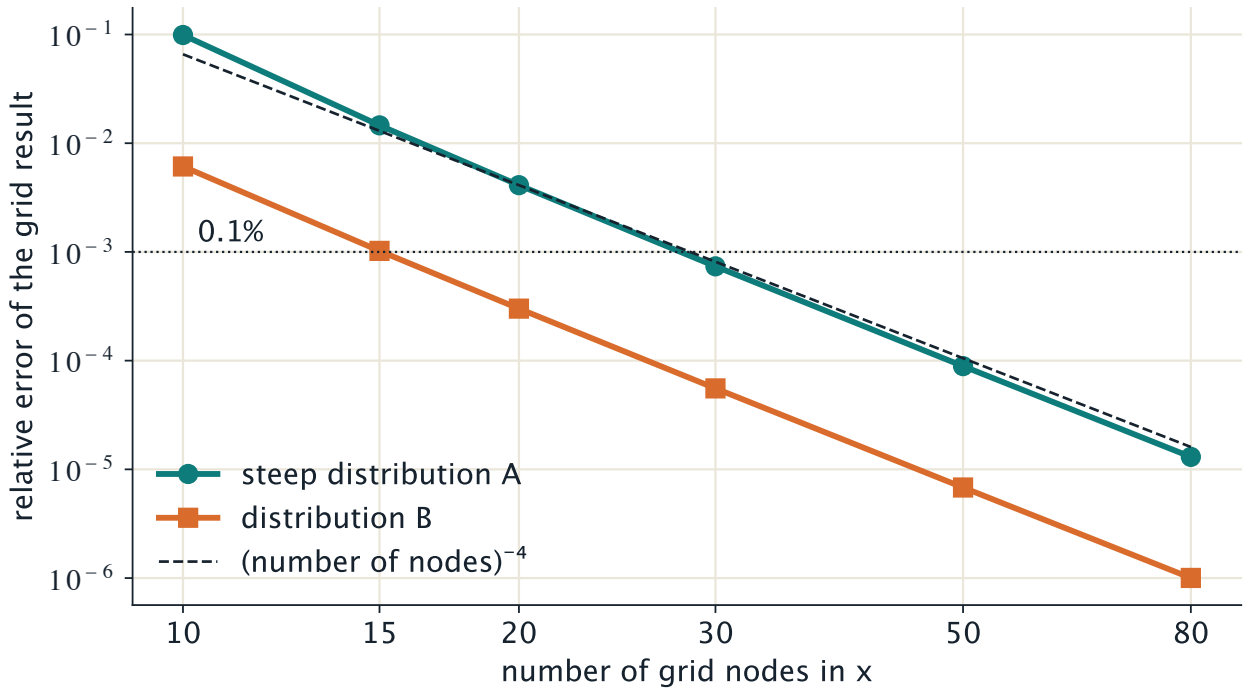

Figure 4. Accuracy of Eqs. (3.3.30) and (3.3.31) in a toy (illustrative). A grid is filled once from 200,000 events with cubic interpolation, then used with two distributions that were not involved in filling it, and compared with the direct sum over the same events. The error is from interpolation alone and falls as the fourth power of the node spacing.

Numbers. In the toy of Figure 4, with nodes between $x = 10^{-3}$ and 1, a steep distribution $\propto x^{-1.2}(1-x)^3$ is reproduced to 0.4% with 20 nodes, 0.07% with 30 and 0.009% with 50. The Snowmass report quotes 0.1% as typical for production grids [3]. The nodes are spaced evenly in a function $y(x)$ chosen to put them where the PDFs vary fastest [3].

Scales, two hadrons and orders

The full object adds three things [3]. The scale is interpolated on nodes μ_k in the same way. Each order in α_S is stored separately, labelled by the total power p of the coupling, so that the coupling can be changed afterwards. And for two incoming hadrons there are two momentum fractions:

$$\begin{aligned} \sigma &\approx \sum_{p} \sum_{\lambda} \sum_{i,j,k} \left(\frac{\alpha_S(\mu_k)}{2\pi}\right)^p F_\lambda(x_i, x_j, \mu_k)\, \hat{\sigma}^{(p)}_{\lambda,ijk}, \\ F_\lambda(x_i, x_j, \mu_k) &= \sum_{(a,b)\in\lambda} f_a(x_i, \mu_k)\, f_b(x_j, \mu_k). \end{aligned} \tag{3.3.32}$$

With eleven partons, top excluded, there are $11 \times 11 = 121$ pairs (a, b). Symmetries of the hard process group them into a few *parton luminosities* F_λ: for jet production, 13 [3]. Further terms, logarithmic in the scales, allow the scales

to be varied afterwards.

An FK table is Eq. (3.3.32) with the PDFs at μ_k replaced by the evolution operator acting on the PDFs at Q_0 (chapter 1.5, section 3). The grid accepts any PDF, α_S and scale choice. The FK table gives that freedom up for speed.

The tools

TOOL	WHAT IT DOES	FROM THE SNOWMASS REPORT [3]
LHAPDF	delivers published PDFs to any code	version 6 since 2013; more than 1150 sets; values on a grid, interpolated by local cubics in $\ln x$ and $\ln Q^2$
APPLgrid, fastNLO	interpolation grids for QCD	independent implementations of the grid technique; interfaced to NNLO jet calculations
PineAPPL	interpolation grids for any orders	arbitrary powers of α_S and α, so electroweak corrections fit; converts the two older formats
EKO	evolution operators	full evolution to NNLO; combined with PineAPPL grids to make FK tables
xFitter	open-source fitting framework	the first public fit code, successor of the HERAPDF code; fits to NNLO, profiling and reweighting
NNPDF code	open-source fitting framework	the complete NNPDF4.0 machinery, with data, theory tables and validation tools

The papers that introduced these tools are collected in [13]. Two remarks on the table.

- **Delivery is itself an interpolation.** A published set is a table of values, and a user's cross-section inherits the accuracy of the interpolation between them. The default cubic interpolation was found insufficiently stable for N³LO calculations, and smoother interpolators were developed in response [3].
- **Open code changed what can be checked.** Until recently only the output tables of a fit were public. With the codes released, a result can be reproduced and differences between groups traced to their cause [3, 10]. This project runs on NNPDF's public data and theory tables.

10. Where this meets our fits

Every number here is from the project ledgers.

- **Cuts and target mass.** The Phase B fits apply $Q^2 > 3.49\ \mathrm{GeV}^2$ and $W^2 > 12.5\ \mathrm{GeV}^2$, and theory 40000000 has target-mass corrections switched on. Section 2 is the content of that switch: the cut removes the region where the correction is large, and the correction handles what remains. No higher-twist term is fitted.
- **Deuteron data.** Phase A used 648 points after cuts: 33 and 333 on protons from SLAC and BCDMS, and 34 and 248 on deuterons. So 282 of the 648 points depend on Eq. (3.3.8). The grid-model fit that reached only $\chi^2/N_{\mathrm{dat}} = 5.84$ on these data (PPDF-9) raised the question of whether missing higher-twist or deuteron corrections were responsible. They were not: the MSHT20 form fitted the same data, with the same theory, to $\chi^2/N_{\mathrm{dat}} = 1.002$ (PPDF-12), and the ledger attributes the earlier floor to the rigidity of the model.

- **Fixed order.** The theory is NNLO with no resummation. Sections 4 to 6 say where that is exposed: the largest-x fixed-target points, and the HERA points at the smallest x and lowest Q^2.
- **Grids.** The staged theory holds 254 PineAPPL grids, and the global Phase B fit uses 101 hadronic FK tables. A missing grid stops a physics question outright: PPDF-37, the test of whether targeted strangeness data (W +charm) would cure the eight remaining flat directions, is blocked because no current theory ships a grid for that process.
- **Learning methods.** Colibri evaluates Eq. (3.3.27) with a 52-parameter form in place of a network, in JAX, with an automatically differentiable likelihood. On the global data set it reaches $\chi^2/N_{\rm dat} = 1.2380$ against the 1.17 of NNPDF4.0, which the ledger records as 1.058 times that value (PPDF-35). The state file warns against setting the 52 parameters beside NNPDF's 763, which are regularised network weights.

Derivations

D1. A massless quark in a massive proton

Derives (3.3.4), (3.3.5)

The vectors. Let p and n be light-like with $n \cdot p = 1$. Then $P = p + \frac{1}{2}M^2 n$ has $P^2 = M^2$. The vectors P and q span a plane, and p and n can be chosen in it, so $q = a\,p + b\,n$ with no transverse part. The struck quark has $k = \xi p$.

Two conditions. $q^2 = 2ab = -Q^2$. The outgoing quark is massless: $(\xi p + q)^2 = 2\xi b - Q^2 = 0$. Hence $b = Q^2/2\xi$ and $a = -\xi$, which is Eq. (3.3.3).

The Nachtmann variable. $\nu = P \cdot q = b + \frac{1}{2}M^2 a = Q^2/2\xi - \frac{1}{2}\xi M^2$, so $\xi^2 M^2 + 2\nu\xi - Q^2 = 0$. With $\nu = Q^2/2x$ the positive root is

$$\xi = \frac{-\nu + \sqrt{\nu^2 + M^2 Q^2}}{M^2} = \frac{Q^2}{2xM^2}\,(r-1) = \frac{2x}{1+r},$$

using $r^2 - 1 = 4x^2M^2/Q^2$. This is Eq. (3.3.4). The same relation gives $\xi^2 M^2/Q^2 = (r-1)/(r+1)$ and therefore

$$1 + \frac{\xi^2 M^2}{Q^2} = \frac{2r}{1+r} = \frac{\xi\, r}{x}.$$

The tensor. As in chapter 1.4, the proton's tensor is the quark's, weighted by $q(\xi')\,d\xi'/\xi'$, the weight that reproduces Eq. (1.4.1) when $M = 0$. Its ingredients are the spin-averaged trace $w^{\alpha\beta} = \frac{1}{2}\mathrm{Tr}[\not{k}\gamma^\alpha \not{k}'\gamma^\beta] = 2\big[k^\alpha k'^\beta + k'^\alpha k^\beta - g^{\alpha\beta} k\cdot k'\big]$ with $k' = k + q$, the factor $1/4\pi$, and the phase space $2\pi\,\delta\big((\xi' p + q)^2\big) = 2\pi\,\delta(\xi' - \xi)/2p\cdot q$. For one flavour of unit charge,

$$W^{\alpha\beta} = \frac{q(\xi)}{4\,\xi\, p\cdot q}\; w^{\alpha\beta} = \frac{q(\xi)}{2Q^2}\; w^{\alpha\beta},$$

since $p \cdot q = b = Q^2/2\xi$.

Rewriting the trace. Let $\hat{k} = k + \frac{1}{2}q$. It is orthogonal to q, because $k\cdot q = \frac{1}{2}Q^2$ for massless k and k'. Then $k^\alpha k'^\beta + k'^\alpha k^\beta = 2\hat{k}^\alpha\hat{k}^\beta - \frac{1}{2}q^\alpha q^\beta$ and $k\cdot k' = \frac{1}{2}Q^2$, so

$$w^{\alpha\beta} = Q^2\Big(-g^{\alpha\beta} + \frac{q^\alpha q^\beta}{q^2}\Big) + 4\,\hat{k}^\alpha\hat{k}^\beta.$$

Relating the two hatted vectors. From Eq. (3.3.3), $n = (2\xi/Q^2)(q + \xi p)$, so $P = \left(1 + \xi^2 M^2/Q^2\right) p + (\xi M^2/Q^2)\, q$. Removing the parts along q, $\hat{P} = (1 + \xi^2 M^2/Q^2)\, \hat{k}/\xi$, that is, $\hat{k} = (x/r)\, \hat{P}$.

Reading off. Comparing with the tensor decomposition of chapter 1.1, section 6, $W^{\alpha\beta} = (-g^{\alpha\beta} + q^\alpha q^\beta/q^2) F_1 + \hat{P}^\alpha \hat{P}^\beta F_2/\nu$: $F_1 = \frac{1}{2} q(\xi)$, and $F_2/\nu = \left(q(\xi)/2Q^2\right) \cdot 4x^2/r^2$, so $F_2 = x\, q(\xi)/r^2$. Restoring charges and flavours gives Eq. (3.3.5), and $r^2 F_2 - 2xF_1 = 0$.

D2. The deuteron correction and the ratio of down to up

Derives (3.3.10)

The ratio. With isospin symmetry and no sea, $F_2^p = x\left(\frac{4}{9}u + \frac{1}{9}d\right)$ and $F_2^n = x\left(\frac{4}{9}d + \frac{1}{9}u\right)$. Dividing gives the first form of Eq. (3.3.9), and solving $R\,(4 + t) = 1 + 4t$ for $t = d/u$ gives the second.

The slope. Differentiating, $dt/dR = \big[4(4 - R) + (4R - 1)\big]/(4 - R)^2 = 15/(4 - R)^2$.

The correction. Solving Eq. (3.3.8) for the neutron, $R = 2F_2^d/(c\, F_2^p) - 1$. At fixed measured F_2^d and F_2^p, $\delta R = -(1 + R)\, \delta c/c$.

Together. $\delta t = -15\,(1 + R)/(4 - R)^2 \cdot \delta c/c$. Dividing by t gives Eq. (3.3.10). For $t = 0.2$: $R = 1.8/4.2 = 0.429$, and the coefficient is $15 \times 1.429/(3.571^2 \times 0.2) = 8.4$.

D3. Moments of the threshold logarithms

Derives (3.3.12), (3.3.13)

The simple plus distribution. By Eq. (1.4.13), $\int_0^1 dz\, z^{N-1} [1/(1 - z)]_+ = \int_0^1 dz\, (z^{N-1} - 1)/(1 - z)$. For integer N, $(1 - z^{N-1})/(1 - z) = \sum_{k=0}^{N-2} z^k$, whose integral is $\sum_{k=1}^{N-1} 1/k = S_1(N - 1)$. The result is $-S_1(N - 1)$.

A generating function. Consider $I(\epsilon) = \int_0^1 dz\, (z^{N-1} - 1)(1 - z)^{-1+\epsilon} = B(N, \epsilon) - 1/\epsilon$, with B the Euler Beta function. Its expansion in ϵ generates the moments of $[\ln^k(1 - z)/(1 - z)]_+$: the coefficient of $\epsilon^k/k!$.

Expanding. $B(N, \epsilon) = \Gamma(N)\Gamma(\epsilon)/\Gamma(N + \epsilon)$. Using $\Gamma(\epsilon) = \Gamma(1 + \epsilon)/\epsilon$ and $\Gamma(N + \epsilon)/\Gamma(N) = \Gamma(1 + \epsilon) \prod_{k=1}^{N-1} (1 + \epsilon/k)$,

$$B(N, \epsilon) = \frac{1}{\epsilon} \prod_{k=1}^{N-1} \left(1 + \frac{\epsilon}{k}\right)^{-1} = \frac{1}{\epsilon} \exp\Big[-\epsilon S_1 + \tfrac{1}{2}\epsilon^2 S_2 - \dots \Big] = \frac{1}{\epsilon} - S_1 + \frac{\epsilon}{2}\big(S_1^2 + S_2\big) + \dots,$$

with $S_j = S_j(N - 1)$. The term of order ϵ^0 reproduces the first line of Eq. (3.3.12) and the term of order ϵ gives the second.

The coefficient function. Apply Eq. (3.3.12) to the coefficient function of chapter 1.6, section 5. The two plus distributions give $C_F\big[S_1^2 + S_2 + \frac{3}{2} S_1\big]$. The moments of the regular terms vanish as $N \to \infty$, since each integrand is bounded by a constant times $z^{N-1}\,[1 + |\ln(1 - z)|]$. The δ function gives $-C_F(\pi^2/3 + \frac{9}{2})$. With $S_1 \to \ln \bar{N}$ and $S_2 \to \pi^2/6$ the constants combine to $\pi^2/6 - \pi^2/3 - \frac{9}{2}$, which is Eq. (3.3.13).

D4. The anomalous dimension from the characteristic function

Derives (3.3.17), (3.3.18)

Two statements about one function. By ESW's Eq. (4.217), the component of the gluon density with scale dependence $(Q^2)^\gamma$ behaves in x as $x^{-\bar{\alpha}_S \chi(\gamma)}$. In their derivation the transform is taken in the squared transverse size

b^2 of a colour dipole, as $(b^2)^\gamma$ in their Eq. (4.215); identifying the scale with Q^2 is the step taken here. The DGLAP equation at fixed coupling says that the moment N, which is the component $x^{-(N-1)}$ of $x\,g$, behaves in the scale as $(Q^2)^{\gamma(N)}$.

Consistency. A double power $x^{-\omega}(Q^2)^\gamma$ satisfies the first if $\omega = \bar\alpha_S\chi(\gamma)$ and the second if $\omega = N-1$ and $\gamma = \gamma(N)$. For the leading logarithms, which both equations contain, both must hold. That is Eq. (3.3.17). Its output confirms the identification: the series below starts with the known leading-order pole and reproduces ESW's fourth-order coefficient to 0.2% (519.3 against the printed 518.4). Of its two solutions the one with $\gamma \to 0$ as $N \to \infty$ is the perturbative one.

The expansion of the characteristic function. From $\psi(1+\gamma) = \psi(\gamma) + 1/\gamma$ and the series $\psi(1+\gamma) = -\gamma_E + \sum_{k\geq 2}(-1)^k\zeta(k)\gamma^{k-1}$,

$$-\psi(\gamma) - \psi(1-\gamma) = \frac{1}{\gamma} + 2\gamma_E + 2\zeta(3)\gamma^2 + 2\zeta(5)\gamma^4 + \dots$$

The even zeta values cancel between the two terms. Adding $2\psi(1) = -2\gamma_E$ gives Eq. (3.3.16).

Inversion. Write $t = \bar\alpha_S/(N-1)$. Equation (3.3.17) is $\gamma = t\,\phi(\gamma)$ with $\phi(\gamma) = \gamma\chi(\gamma) = 1 + 2\zeta(3)\gamma^3 + 2\zeta(5)\gamma^5 + \dots$ Iterating from $\gamma = t$: the first correction is $2\zeta(3)t^4$; then $2\zeta(5)t^6$; and inserting $\gamma = t + 2\zeta(3)t^4$ into $2\zeta(3)t\gamma^3$ gives a further $2\zeta(3)\cdot 3\cdot 2\zeta(3)\,t^7 = 12\,\zeta(3)^2 t^7$. That is Eq. (3.3.18). There are no terms in t^2, t^3 or t^5 because ϕ has no terms in γ, γ^2 or γ^4.

Normalisation. $\bar\alpha_S = 2C_A\cdot\alpha_S/2\pi$, so t^4 is $(2C_A)^4(\alpha_S/2\pi)^4/(N-1)^4$. One factor of $\alpha_S/2\pi$ is the prefactor of the evolution equation. By Eq. (3.3.15), $1/(N-1)^4$ is the transform of $\ln^3(1/x)/(3!\,x)$. The coefficient of $(\alpha_S/2\pi)^3\ln^3(1/x)$ in $x\,P_{gg}$ is therefore $2\zeta(3)(2C_A)^4/3!$.

The branch point. Near $\gamma = \frac12$, $\chi(\gamma) \approx 4\ln 2 + \frac12\chi''(\frac12)(\gamma-\frac12)^2$ with $\chi'' > 0$. Equation (3.3.17) then gives $\gamma - \frac12 \propto -\sqrt{N-1-\lambda}$, a square-root singularity at $N = 1+\lambda$.

D5. Space-like correlators and the reach in Ioffe time

Derives (3.3.23), (3.3.26)

The decomposition. After the spin average, the matrix element on the left of Eq. (3.3.22) is a four-vector that depends only on P and z. It is therefore a combination of P^μ and z^μ with coefficients that are functions of the invariants $P\cdot z$ and z^2. Nothing has been assumed about z^2.

The light cone. Put $z = \lambda n$ and contract with n_μ. Since $n\cdot P = 1$, $n\cdot z = 0$, $z^2 = 0$ and $\nu = \lambda$, the right-hand side is $2\mathcal{M}(\lambda, 0)$. The definition of chapter 1.3, section 7, $q(x) = \int \frac{d\lambda}{4\pi} e^{i\lambda x}\langle P|\bar\psi(0)\not{n}\,\mathcal{W}\,\psi(\lambda n)|P\rangle$, then reads $q(x) = \int \frac{d\lambda}{4\pi} e^{i\lambda x}\,2\mathcal{M}(\lambda,0)$, which is Eq. (3.3.23). Inverting, $\mathcal{M}(\nu,0) = \int dx\, e^{-i\nu x} q(x)$, whose Taylor coefficients at $\nu = 0$ are the moments.

Equal time. Put $z = (0,0,0,z_3)$ and take $\mu = 0$. Then $z^0 = 0$ removes $\mathcal{N}$, and $\nu = P\cdot z = -P_z z_3$, $z^2 = -z_3^2$.

The cut-off. Insert $\mathcal{M}(\nu,0) = \int dx' e^{-i\nu x'} q(x')$ into Eq. (3.3.23) with the ν integral restricted to $|\nu| < \nu_{\max}$:

$$q_{\rm rec}(x) = \int dx'\, q(x') \int_{-\nu_{\max}}^{\nu_{\max}} \frac{d\nu}{2\pi}\, e^{i\nu(x-x')} = \int dx'\, q(x')\, \frac{\sin[\nu_{\max}(x-x')]}{\pi(x-x')}.$$

The kernel has a central peak between its first zeros at $x - x' = \pm\pi/\nu_{\max}$ and tends to $\delta(x-x')$ as $\nu_{\max}\to\infty$. Features of q narrower than $\pi/\nu_{\max}$ are not resolved.

D6. The interpolation grid

Derives (3.3.30), (3.3.31)

Removing the distribution from the integral. Insert Eq. (3.3.29) in $\sigma = \int dx\, f(x)\hat{\sigma}(x)$. The values $f(x_i)$ are constants, so $\sigma \approx \sum_i f(x_i) \int dx\, E_i(x)\hat{\sigma}(x)$, which is Eq. (3.3.30). The only approximation is the interpolation of f. $\hat{\sigma}$ is not interpolated, and may be a distribution with δ functions and plus prescriptions.

Filling. A Monte Carlo integration estimates $\int dx\, h(x)\, \hat{\sigma}(x) \approx \sum_m w_m\, h(x_m)$ for any smooth h, with weights w_m that include the matrix element, the phase-space measure and the cuts. With $h = f$ this is the direct calculation. With $h = E_i$ it is Eq. (3.3.31). The two agree: $\sum_i f(x_i) g_i = \sum_m w_m \sum_i f(x_i) E_i(x_m) \approx \sum_m w_m f(x_m)$.

The error. The difference between the grid result and the direct sum is $\sum_m w_m \big[f(x_m) - \sum_i f(x_i) E_i(x_m) \big]$: the interpolation error of f, averaged over the events. For polynomial interpolation of degree d on nodes of spacing h it is of order h^{d+1}. Cubic interpolation gives h^4; in the toy of Figure 4 the fitted power between 20 and 80 nodes is 4.15. The Monte Carlo error is common to both sides and cancels.

The condition on the interpolating functions. $\sum_i E_i(x) = 1$ makes a constant f exact, so the total weight $\sum_i g_i = \sum_m w_m$ is preserved whatever the nodes.

References

1. R. K. Ellis, W. J. Stirling and B. R. Webber, *QCD and Collider Physics*, Cambridge University Press (1996), section 4.6. Open access under CC BY-NC 4.0, doi:10.1017/CBO9780511628788. Source for the characteristic function (Eqs. 4.214–4.226), the HERA results quoted in section 6 and the saturation estimate (Eq. 4.228). The wording, derivations and figures are our own.
2. J. M. Moore, *Parton Distributions in Beyond the Standard Model Theories*, PhD thesis, University of Cambridge, sections 1.1.7, 1.2, 1.3, 4.2 and 4.3.
3. S. Amoroso et al., “Snowmass 2021 whitepaper: Proton structure at the precision frontier”, arXiv:2203.13923, sections I C, III B, III E, IV A, IV D, IV F, V C, VI, VII and IX. The source for every statement about the present state of the field in this chapter.
4. A. Accardi, L. T. Brady, W. Melnitchouk, J. F. Owens and N. Sato, Phys. Rev. D 93 (2016) 114017, arXiv:1602.03154; S. Bailey, T. Cridge, L. A. Harland-Lang, A. D. Martin and R. S. Thorne, Eur. Phys. J. C 81 (2021) 341, arXiv:2012.04684.
5. R. D. Ball, E. R. Nocera and R. L. Pearson, Eur. Phys. J. C 81 (2021) 37, arXiv:2011.00009; A. Accardi, T. J. Hobbs, X. Jing and P. M. Nadolsky, Eur. Phys. J. C 81 (2021) 603, arXiv:2102.01107.
6. G. F. Sterman, Nucl. Phys. B 281 (1987) 310; M. Bonvini et al., JHEP 09 (2015) 191, arXiv:1507.01006.
7. E. A. Kuraev, L. N. Lipatov and V. S. Fadin, Sov. Phys. JETP 44 (1976) 443 and 45 (1977) 199; I. I. Balitsky and L. N. Lipatov, Sov. J. Nucl. Phys. 28 (1978) 822; A. H. Mueller, Nucl. Phys. B415 (1994) 373.
8. R. D. Ball, V. Bertone, M. Bonvini, S. Marzani, J. Rojo and L. Rottoli, Eur. Phys. J. C 78 (2018) 321, arXiv:1710.05935; H. Abdolmaleki et al. (xFitter Developers’ Team), Eur. Phys. J. C 78 (2018) 621, arXiv:1802.00064; M. Bonvini, S. Marzani and C. Muselli, JHEP 12 (2017) 117, arXiv:1708.07510.
9. X. Ji, Phys. Rev. Lett. 110 (2013) 262002, arXiv:1305.1539; A. V. Radyushkin, Phys. Rev. D 96 (2017) 034025, arXiv:1705.01488; M. Constantinou et al., Prog. Part. Nucl. Phys. 121 (2021) 103908, arXiv:2006.08636.

10. R. D. Ball et al. (NNPDF), Eur. Phys. J. C 82 (2022) 428, arXiv:2109.02653; R. D. Ball et al. (NNPDF), Eur. Phys. J. C 81 (2021) 958, arXiv:2109.02671; S. Carrazza and J. Cruz-Martinez, Eur. Phys. J. C 79 (2019) 676, arXiv:1907.05075.
11. S. Iranipour and M. Ubiali, JHEP 05 (2022) 032, arXiv:2201.07240.
12. S. Carrazza, J. I. Latorre, J. Rojo and G. Watt, Eur. Phys. J. C 75 (2015) 474, arXiv:1504.06469; S. Carrazza, J. M. Cruz-Martinez and T. R. Rabemananjara, Eur. Phys. J. C 81 (2021) 530, arXiv:2104.04535.
13. A. Buckley et al., "LHAPDF6: parton density access in the LHC precision era", Eur. Phys. J. C 75 (2015) 132, arXiv:1412.7420; T. Carli et al., "A posteriori inclusion of parton density functions in NLO QCD final-state calculations at hadron colliders: the APPLGRID project", Eur. Phys. J. C 66 (2010) 503, arXiv:0911.2985; D. Britzger et al., Eur. Phys. J. C 79 (2019) 845, arXiv:1906.05303; S. Carrazza, E. R. Nocera, C. Schwan and M. Zaro, JHEP 12 (2020) 108, arXiv:2008.12789; S. Alekhin et al., Eur. Phys. J. C 75 (2015) 304, arXiv:1410.4412.